INTERNATIONAL JOURNAL FOR NUMERICAL METHODS IN FLUIDS
Int. J. Numer. Meth. Fluids 2004; **45**:321–340 (DOI: 10.1002/fld.703)

A non-linear dynamical system approach to finite amplitude Taylor-Vortex flow of shear-thinning fluids

Zhenyu Li and Roger E. Khayat*,†

Department of Mechanical and Materials Engineering, University of Western Ontario, London, Ontario, N6A 5B9, Canada

SUMMARY

The effect of shear thinning on the stability of the Taylor–Couette flow is explored for a Carreau–Bird fluid in the narrow-gap limit. The Galerkin projection method is used to derive a low-order dynamical system from the conservation of mass and momentum equations. In comparison with the Newtonian system, the present equations include additional non-linear coupling in the velocity components through the viscosity. It is found that the critical Taylor number, corresponding to the loss of stability of the circular Couette flow, becomes lower as the shear-thinning effect increases. That is, shear thinning tends to precipitate the onset of Taylor vortex flow, which coincides with the onset of a supercritical bifurcation. Comparison with existing measurements of the effect of shear thinning on the critical Taylor and wave numbers show good agreement. The Taylor vortex cellular structure loses its stability in turn, as the Taylor number reaches a critical value. At this point, an inverse Hopf bifurcation emerges. In contrast to Newtonian flow, the bifurcation diagrams exhibit a turning point that sharpens with shear-thinning effect. Copyright © 2004 John Wiley & Sons, Ltd.

KEY WORDS: Taylor–Couette flow; shear thinning; Galerkin projection method; Hopf bifurcation

1. INTRODUCTION

The interplay between inertia and shear thinning effects is examined for axisymmetric Taylor–Couette flow (TCF) in the narrow-gap limit. Shear thinning is an inherent property of polymeric fluids used in materials processing. The rate of shearing during a polymer process can be high enough for the viscosity to change typically by a factor of 1000. It is therefore not realistic to assume that the viscosity, which is directly related to the rate of strain, be constant as in the Newtonian case. However, the presence of a rate-of-strain dependent viscosity gives rise to additional non-linearities (in addition to inertia) and coupling among the flow variables.

*Correspondence to: Roger E. Khayat, Department of Mechanical and Materials Engineering, University of Western Ontario, London, Ontario, N6A 5B9, Canada.
†E-mail: rkhayat@eng.uwo.ca

Received 30 July 2002
Revised 6 October 2003

Similar to any flow in the transition regime, the TCF of non-Newtonian fluids involves a continuous range of excited spatio-temporal scales. In order to assess the effect of the smaller length scales on the flow, a high resolution of the flow field is needed. It is by now well established that low-order dynamical systems can be a viable alternative to conventional numerical methods in the weakly non-linear range of flow [1, 2]. Despite the severe degree of truncation in the formulation of these models, some of the basic qualitative elements of the onset of Taylor vortices and destabilization of the cellular structure have been recovered using low-order dynamical systems.

Kuhlmann [3] and later Kuhlmann *et al.* [4] examined the stationary and time-periodic Taylor vortex flow (TVF), in the narrow gap limit and arbitrary gap width, respectively, with the inner cylinder rotating at a constant and harmonically modulated angular velocity. The solution to the full Navier–Stokes equations was obtained by implementing a finite-difference scheme, and an approximate approach based on the Galerkin representation. Comparison of flows based on the two methods led to good agreement. A severe truncation level was used, leading to a three-dimensional system, which turned out to be the Lorenz system with the Prandtl number equal to unity. In this case, the model cannot predict the destabilization of the Taylor vortices, and therefore cannot account for the onset of chaotic behaviour.

Although dynamical systems have been mainly formulated for Newtonian fluids [3, 4], they have recently been applied to non-Newtonian fluids to explore the onset of thermal convection [5–8], Taylor vortex flow [9–12], and secondary channel flow [13, 14]. The effect of weak shear thinning in thermal convection [8] and TCF [12] was examined using truncation levels similar to that leading to the Lorenz model [2]. Despite the severe level of truncation, the low-order dynamical system approach yielded a good agreement with experiments in some cases, such as the TCF of highly elastic polymeric solutions, often designated as Boger fluids [9–11].

The interplay between inertia and elasticity in TCF was first examined using a system of only six degrees of freedom [9]. The influence of higher-order modes, stemming mainly from normal stress effects, was then investigated for purely elastic fluids without inertia [10]. The finite amplitude elastic overstability (in the absence of inertia), which is usually observed in experiment [15], was accurately predicted for axisymmetric TVF of the Boger fluids [16] in the narrow-gap limit. The model predicts, as experiment suggests, the onset of overstability, the growth of oscillation amplitude of flow, and the emergence of higher harmonics in the power spectrum as fluid elasticity increases beyond a critical level. Also good agreement was obtained upon comparison with the exact results from linear stability analysis [17]. More recently, the effects of both inertia and elasticity were examined for a Boger fluid [11]. Most of the dynamics observed during the experiments of Baumert and Muller [18, 19] was recovered by the theory.

In this paper, the influence of shear thinning on TCF is examined by adopting a non-linear dynamical system approach. Although the present study uses the Carreau–Bird model [16] for the viscosity dependence on the rate of strain, and thus is primarily concerned with high-molecular-weight fluids, it is also of relevance to shear-thinning fluids in general, even for some simple (monatomic) fluids. Using the method of non-equilibrium molecular dynamics, several authors [20–22] have shown that even a simple fluid like liquid Argon can exhibit rheologically complex behaviour. Ashurst and Hoover [20] directly integrated the microscopic equations governing the dynamics of 108 particles. They predicted that the viscosity of the non-equilibrium fluid system decreases as the shear rate increases. At higher shear rate ranges, a phase transition was observed by Erpenbeck [21], which led the system to undergo a two-

dimensional ordering. Heyes [22] related the rheological behaviour of the flow to the dynamics of molecular interactions to investigate the cause of shear thinning in simple fluids. Based on the kinetic theory of simple dense fluids, Eu [23] and Bhattacharya and Eu [24] examined the shear-rate and frequency dependence of viscosity for a dense Lennard-Jones fluid, and compared their results with the molecular dynamics simulation of Evans [25]. Generally, the kinetic theory foundation of constitutive models for monatomic dilute (dense) simple fluids, based on the solution of the generalized Boltzmann equation, clearly reflects the non-Newtonian character of such fluids [26–28]. The major distinction in constitutive behaviour between these monatomic fluids and polyatomic liquids appears to be the form of transport coefficients in the limit of zero-shear-rate range [29]. The non-Newtonian character, inherent to other simple fluids such as rarefied gases, can also be inferred from the kinetic theory of Grad's 13-moment method [30].

The present study isolates the effect of shear thinning from that of fluid elasticity. The reader is referred to the review by Larson [31] for a general overview of viscoelastic instability. The study, however, is not so much concerned with the emergence of shear-thinning overstability, as it focuses more on the interplay between inertia and shear thinning, and therefore on the departure from Newtonian behaviour. The critical Taylor number at the onset of the Taylor vortex cellular structure is expected to be lower than that for a Newtonian fluid as a result of the decrease in viscous effects. One also expects, similarly to Newtonian flow [3], where two steady-state branches emerge at the onset of a supercritical bifurcation at a critical Taylor number, that the nature and magnitude of these branches to depend strongly on shear thinning. The question arises then as to whether these branches lose their stability, in turn, (for instance, via a Hopf bifurcation) as the Taylor number exceeds another critical value as a result of shear thinning. This is found to be the case for the thermal convection of shear-thinning fluids [8]. In contrast, and on the basis of the low-order approach, the TVF does not lose its stability in the case of Newtonian fluids.

Ashrafi and Khayat [12] examined the influence of shear thinning on the TCF. However, their results were based on the unrealistic free (slip) boundary condition. A severe level of truncation as in References [3, 8, 9], was adopted in the Fourier representation for the flow field. Such levels of truncation have also been widely used for the Navier–Stokes and energy equations [32, 33]. Examination of the influence of additional modes [34–36] indicated that many of the gross features predicted by low-order models are essentially recovered by higher-order models.

Crumeyrolle *et al.* [37] carried out measurements on the Taylor–Couette flow to study the inertial and elastic modes in dilute and semidilute solutions of high-molecular-weight polyethyleneoxide in water. Both shear-thinning and elastic effects were considered. The shear-thinning behaviour of the solutions was determined through low-shear-viscosity measurements. They found that solutions with concentrations larger than 150 ppm exhibit a clear shear-thinning behaviour, which is well represented by the Carreau–Bird model. Depending on the solute concentration, different flow structures can appear at the onset of instability. For dilute concentrations, the critical mode corresponds to the stationary and axisymmetric Taylor vortex flow, which bifurcates to time periodic wavy vortex flow for a higher shear rate. The oscillation amplitude of periodic vortex flow decreases with shear rate. For semi-dilute solutions, the critical mode occurs in the form of standing wave, the frequency of which decreases with shear rate. The critical Taylor number increases for solutions without a shear-thinning effect and decreases for solutions exhibiting shear thinning.

Yi and Kim [38] investigated the effects of both the shear rate dependent viscosity and the first and second normal stress differences on the critical Taylor number in dilute polymer solutions. The polymer chosen in their study is polyacrylamide, xanthan gum and polyacrylic acid, and the solvent is a 1:1 mixture of glycerine and distilled water. Their results show that the qualitative characteristics of transition from the stable Couette flow to the turbulent flow are similar to those of Newtonian fluids. In the case of polyacrylamide and xanthan gum solutions, the critical Taylor number decreases as the polymer concentration increases. Even a very weak shear rate dependency of viscosity was found to play an important role in determining the stability of the Taylor–Couette flow.

Sinevic *et al.* [39] determined the torque for both Newtonian and essentially inelastic shear-thinning fluids in TCF in both narrow- and wide-gap geometries. Results showed that the critical Taylor number is strongly dependent on the degree of shear thinning. Escudier *et al.* [40] investigated the flow structure in a Taylor–Couette geometry with a radius ratio of 0.506. Two types of shear-thinning fluids, namely an aqueous solution of Xanthan gum and a Laponite/CMC aqueous blend, were used in their experiments. They found that the shear-thinning aspect of the fluid rheology for both non-Newtonian fluids was far more significant than either thixotropy or viscoelasticity.

In the present study, shear-thinning effect is examined in the linear and non-linear range using the more realistic rigid boundary conditions. A modal assessment is carried out to secure convergence. A relatively large number of modes are used. The problem is formulated in Section 2, where the perturbation equations for a Carreau–Bird model are derived using the Galerkin projection method. Linear stability analysis is then carried out, and the post-critical bifurcation diagrams are computed in Section 3. Concluding remarks are given in Section 4.

2. PROBLEM FORMULATION

The dynamical system for a Carreau–Bird fluid is derived in this section. The general equations for a shear-thinning fluid are first derived in the narrow gap limit. The dynamical system is then obtained using the Galerkin projection method. A linear stability analysis is carried out involving an arbitrary number of modes to ensure the reliability of the dynamical system.

2.1. Governing equations in the narrow-gap limit

Consider the flow of an incompressible shear-thinning fluid between two infinite, coaxial cylinders of inner and outer radii R_1 and R_2, respectively. The inner cylinder is assumed to rotate at a constant angular velocity, Ω. The outer cylinder is assumed to be at rest. In this case, the flow is governed by the following conservation of mass and linear momentum equations for an incompressible fluid,

$$\nabla \cdot \mathbf{U} = 0 \tag{1}$$

$$\rho \left(\frac{\partial \mathbf{U}}{\partial T} + \mathbf{U} \cdot \nabla \mathbf{U} \right) = \nabla \cdot \boldsymbol{\tau} - \nabla P \tag{2}$$

where $\mathbf{U}=(U_R, U_\Theta, U_Z)^T$ is the velocity vector in the cylindrical co-ordinates (R,Θ,Z), with Z taken along the common cylinder axis, T is the time, P is the pressure, $\boldsymbol{\tau}=\mu\dot{\boldsymbol{\gamma}}$ is the shear stress, μ is the shear-rate dependent viscosity, $\dot{\boldsymbol{\gamma}}=\nabla\mathbf{U}+(\nabla\mathbf{U})^{\mathrm{T}}$ is the rate-of-strain tensor, ρ is the density, and ∇ is the three-dimensional gradient operator. The fluid is assumed to have a zero-shear-rate viscosity μ_0. In this study, only axisymmetric flow is considered, so that the dependence on Θ is neglected.

The first step in reducing Equations (1) and (2) to the narrow-gap limit consists of introducing dimensionless co-ordinates, x and z, in the transverse and axial directions, respectively, time t, pressure p, velocity components u_x, u_y, u_z, and viscosity η, as follows:

$$\begin{gathered} x=\frac{2R-(R_1+R_2)}{2D}, \quad z=\frac{Z}{D}, \quad t=\frac{v_0}{D^2}\,T, \quad p=\frac{D^2}{\rho v_0^2}\,P \\ u_x=\frac{D}{v_0}\,U_R, \quad u_y=\frac{1}{R_1\Omega}\,U_\Theta, \quad u_z=\frac{D}{v_0}\,U_Z, \quad \eta=\frac{\mu}{\mu_0} \end{gathered} \tag{3}$$

where $D=R_2-R_1$ is the gap width, and $v_0=\mu_0/\rho$ is the zero-shear-rate kinematic viscosity.

In the present study, the flow is taken as the superposition of the base flow and a perturbation from the base flow. In the narrow-gap limit, the corresponding velocity components $(u_x^0, u_y^0, u_z^0)^{\mathrm{T}}$ and pressure p^0 of the base flow, are given explicitly as

$$u_x^0=u_z^0=0, \quad u_y^0=1/2-x, \quad p_{,x}^0=Ta(1/2-x)^2 \tag{4}$$

in which the Taylor number, Ta, is defined in terms of the Reynolds number, Re, and the gap-to-radius ratio, ε,

$$Ta=Re^2\varepsilon, \quad Re=\frac{\Omega R_1 D}{v_0} \quad \varepsilon=\frac{D}{R_1} \tag{5}$$

In the present work, the Carreau–Bird model is adopted for shear-thinning fluids. A major advantage of this model is that Newton's law of viscosity [16] is recovered in the limit of zero-shear-rate. The general Carreau–Bird viscosity model can be written in dimensionless form

$$\eta(\dot{\gamma})=s+(1-s)[1+(De\dot{\gamma})^2]^{\frac{(n-1)}{2}} \tag{6}$$

where n is the power-law exponent, which is less than 1 for shear-thinning fluids. In the limit $n\to 1$, one recovers the expression for the Newtonian viscosity. Here s is the ratio of the infinite to zero shear-rate viscosities [16], $De=\lambda R_1\Omega/D$ is the Deborah number for the problem, λ being the time constant. Note that the magnitude of the shear rate tensor, $\dot{\gamma}$ is non-dimensionalized with respect to $R_1\Omega/D$ and expressed in terms of the components of the rate-of-strain tensor as [16]

$$\dot{\gamma}=\sqrt{\dot{\gamma}_{xy}^2+\dot{\gamma}_{xz}^2+\dot{\gamma}_{yz}^2+\frac{\varepsilon}{2Ta}(\dot{\gamma}_{xx}^2+\dot{\gamma}_{yy}^2+\dot{\gamma}_{zz}^2)} \tag{7}$$

where $\dot{\gamma}_{ij}=u_{i,j}+u_{j,i}$, with $i,j=x,y,z$. In the present study, it is assumed that $Ta=O(1)$ or higher, so that the terms of $O(\varepsilon/Ta)$ in Equation (7) can be neglected.

The small perturbation from the base flow, u'_x, u'_y, and u'_z, for the velocity components, p' for the pressure, and η' for the viscosity, are defined as

$$u'_x = u_x - u^0_x,\ u'_y = u_y - u^0_y,\ u'_z = u_z - u^0_z,\ p' = p - p^0,\ \eta' = \eta - \eta^0 \tag{8}$$

where, by substituting for $\dot{\gamma}$, the following expressions for η and η^0 can be obtained:

$$\eta = s + (1-s)\{1 + De^2[(u'_{y,x} - 1)^2 + (u'_{x,z} + u'_{z,x})^2 + u'^2_{y,z}]\}^{(n-1)/2} \tag{9a}$$

$$\eta^0 = s + (1-s)[1 + De^2]^{(n-1)/2} \tag{9b}$$

Note that in linear stability analysis the perturbation terms are assumed to be small. Using Equations (3), (4), (8), and neglecting terms of $O(\varepsilon/Ta)$, Equations (1) and (2) reduce to the following form in the narrow-gap limit:

$$u'_{x,x} + u'_{z,z} = 0 \tag{10a}$$

$$u'_{x,t} + u'_x u'_{x,x} + u'_x u'_{x,z} = Tau'^2_y + 2Tau'_y(1/2 - x) + \eta(u'_{x,xx} + u'_{x,zz}) + 2\eta_{,x}u'_{x,x} + \eta_{,z}(u'_{x,z} + u'_{z,x}) - p'_{,x} \tag{10b}$$

$$u'_{y,t} + u'_x u'_{y,x} + u'_z u'_{y,z} = u'_x + \eta(u'_{y,xx} + u'_{y,zz}) + \eta_{,x}(u'_{y,x} - 1) + \eta_{,z}u'_{y,z} \tag{10c}$$

$$u'_{z,t} + u'_x u'_{z,x} + u'_z u'_{z,z} = \eta(u'_{z,xx} + u'_{z,zz}) + \eta_{,x}(u'_{x,x} + u'_{z,x}) + 2\eta_{,z}u'_{z,z} - p'_{,z} \tag{10d}$$

The solution of Equations (10) is considered next using the method of Galerkin projection.

2.2. Galerkin projection and the dynamical system

The Galerkin projection method consists of expanding the velocity and pressure in terms of orthogonal functions of x and z, and projecting Equations (10) onto each mode of the expansion, leading to the equations governing the time-dependent expansion coefficients. Unlike the previous work [12], Fourier modes cannot be used in the x direction. By introducing infinite Fourier series in the z direction and Chandrasekhar functions [41] in the x direction, with the series coefficients depending only on time, the general solution for the axisymmetric TCF can be decomposed as follow:

$$u'_x(x,z,t) = \sum_{n=1}^{\infty}\sum_{m=1}^{\infty} u_{mn}(t)\Phi_n(x)\cos mwz \tag{11a}$$

$$u'_y(x,z,t) = \sum_{n=1}^{\infty}\left[\sum_{m=1}^{\infty} v_{mn}(t)\Phi_n(x)\cos mwz + v_{0n}(t)\Phi_n(x)\right] \tag{11b}$$

$$u'_z(x,z,t) = \sum_{n=1}^{\infty}\sum_{m=1}^{\infty} w_{mn}(t)\Phi_n(x)\sin mwz \tag{11c}$$

$$p'(x,z,t)=\sum_{n=1}^{\infty}\sum_{m=1}^{\infty}p_{mn}(t)\Phi_n(x)\cos mwz \tag{11d}$$

where $u_{mn}(t)$, $v_{0n}(t)$, $v_{mn}(t)$, $w_{mn}(t)$ and $p_{mn}(t)$ are the time dependent coefficients and w is the dimensionless wave number (in units of D) in the z direction. $\Phi_n(x)$ are the Chandrasekhar orthogonal functions [41], which are expressed as

$$\Phi_n(x)=\begin{cases} S_n(x)=\dfrac{\sinh(\mu_n x)}{\sinh(\mu_n/2)}-\dfrac{\sin(\mu_n x)}{\sin(\mu_n/2)}, & n \text{ even} \\ C_{\left(\frac{n+1}{2}\right)}(x)=\dfrac{\cosh(\lambda_{(n+1)/2}x)}{\cosh(\lambda_{(n+1)/2}/2)}-\dfrac{\cos(\lambda_{(n+1)/2}x)}{\cos(\lambda_{(n+1)/2}/2)}, & n \text{ odd} \end{cases} \tag{12}$$

where, μ_n and λ_n are constant coefficients.

The first step in the Galerkin projection method consists of substituting expression (11) into Equations (10), multiplying by the appropriate mode, and integrating over $x\in[-\frac{1}{2},\frac{1}{2}]$ and $z\in[0,\pi/w]$. As a minimal number of modes is kept in the z direction to secure that the non-linear terms are retained for Newtonian flow [32]. The axial velocity component and the pressure are eliminated by the terms of remaining components. The resulting set of non-linear and coupled ordinary differential equations, which govern the time-dependent expansion coefficients, become

$$\begin{aligned} v_{0p,t}=&-\frac{1}{2}\sum_{k=1}^{N}\sum_{i=1}^{N}v_{1k}u_{1i}(\langle\Phi_{k,x}\Phi_i\Phi_p\rangle+\langle\Phi_k\Phi_{i,x}\Phi_p\rangle)+\frac{w}{\pi}\Bigg[\sum_{j=1}^{N}v_{0j}(\langle\langle\eta'\Phi_{j,xx}\Phi_p\rangle\rangle \\ &+\langle\langle\eta'\Phi_{j,xx}\Phi_p\rangle\rangle)+\sum_{k=1}^{N}v_{ik}(\langle\langle\eta'\Phi_{k,xx}\Phi_p\cos wz\rangle\rangle-w^2\langle\langle\eta'\Phi_k\Phi_p\cos wz\rangle\rangle \\ &+\langle\langle\eta'_{,x}\Phi_{k,x}\Phi_p\cos wz\rangle\rangle-w\langle\langle\eta'_{,z}\Phi_k\Phi_p\sin wz\rangle\rangle)\Bigg]-\frac{w}{\pi}\langle\langle\eta'_{,x}\Phi_p\rangle\rangle \end{aligned} \tag{13a}$$

$$\begin{aligned} v_{1p,t}=&-\sum_{k=1}^{N}\sum_{i=1}^{N}v_{0k}u_{1i}(\langle\Phi_{k,x}\Phi_i\Phi_p\rangle)+u_{1p}+\frac{2w}{\pi}\Bigg[\sum_{j=1}^{N}v_{0j}(\langle\langle\eta'\Phi_{j,xx}\Phi_p\cos wz\rangle\rangle \\ &+\langle\langle\eta'_{,x}\Phi_{j,x}\Phi_p\cos wz\rangle\rangle)+\sum_{k=1}^{N}v_{ik}(\langle\langle\eta'\Phi_{k,xx}\Phi_p\cos^2 wz\rangle\rangle-w^2\langle\langle\eta'\Phi_k\Phi_p\cos^2 wz\rangle\rangle \\ &+\langle\langle\eta'_{,x}\Phi_{k,x}\Phi_p\cos^2 wz\rangle\rangle-w\langle\langle\eta'_{,z}\Phi_k\Phi_p\cos wz\sin wz\rangle\rangle)\Bigg]-\frac{2w}{\pi}\langle\langle\eta'_{,x}\Phi_p\cos wz\rangle\rangle \end{aligned} \tag{13b}$$

$$
\begin{aligned}
&\sum_{i=1}^{N} u_{1i,t}(w^2\delta_{ip} - \langle \Phi_{i,xx}\Phi_p \rangle) \\
&\quad = 2w^2 Ta \left(\sum_{k=1}^{N}\sum_{i=1}^{N} v_{0k}v_{1i}\langle \Phi_k\Phi_i\Phi_p\rangle + \sum_{k=1}^{N} v_{1k}\langle (0.5-x)\Phi_k\Phi_p\rangle \right) \\
&\qquad + \frac{2w}{\pi}\sum_{i=1}^{N} u_{1i}(w^2\langle\langle \eta'\Phi_{i,xx}\Phi_p\cos^2 wz\rangle\rangle - w^4\langle\langle \eta'\Phi_i\Phi_p\cos^2 wz\rangle\rangle \\
&\qquad + 2w^2\langle\langle \eta'_{,x}\Phi_{i,x}\Phi_p\cos^2 wz\rangle\rangle - 3w\langle\langle \eta'_{,z}\Phi_{i,xx}\Phi_p\cos wz\sin wz\rangle\rangle \\
&\qquad - w^3\langle\langle \eta'_{,z}\Phi_i\Phi_p\cos wz\sin wz\rangle\rangle - \beta_i^4\langle\langle \eta'\Phi_i\Phi_p\sin^2 wz\rangle\rangle \\
&\qquad + w^2\langle\langle \eta'\Phi_{i,xx}\Phi_p\sin^2 wz\rangle\rangle - 2w\langle\langle \eta'_{,xz}\Phi_{i,x}\Phi_p\cos wz\sin wz\rangle\rangle \\
&\qquad - 2\langle\langle \eta'_{,x}\Phi_{i,xxx}\Phi_p\sin^2 wz\rangle\rangle - \langle\langle \eta'_{,xx}\Phi_{i,xx}\Phi_p\sin^2 wz\rangle\rangle \\
&\qquad - w^2\langle\langle \eta'_{,xx}\Phi_i\Phi_p\sin^2 wz\rangle\rangle \Big)
\end{aligned}
\tag{13c}
$$

where

$$
\beta_i = \begin{cases} \mu_i & i \text{ even} \\ \lambda i & i \text{ odd} \end{cases}, \quad p = 1, 2, \ldots, N.
$$

$\langle\ \rangle$ stands for integration over x, and $\langle\langle\ \rangle\rangle$ stands for double integrate over x and z. In the limit $n \to 1$, Equation (13) reduce to the Newtonian form. Compared to the Newtonian system, Equations (13) are highly non-linear. In addition to the usual non-linearities stemming from inertia effects, there are non-linearities stemming from shear-thinning effects.

The truncation level adopted is determined by carrying out a convergence assessment of the number of modes in the transverse direction (x), in both the linear and non-linear ranges of Taylor number. The situation is typically illustrated by the stability and bifurcation results for a Newtonian fluid. The marginal stability curves are shown in Figure 1 for various values of the number of modes, N. Convergence is essentially attained for $N > 5$. Table I shows the influence of higher-order modes on the values of the critical Taylor number and corresponding wave number. A similar convergence rate is achieved in the non-linear range. Figure 2 shows the bifurcation curves, which correspond to the (steady) TVF, for different levels of truncation.

3. STABILITY AND BIFURCATION ANALYSES

The stability of both the circular Couette flow (CCF) and TVF is examined by exploring some of the fundamental differences between Newtonian and shear-thinning fluids. It turns out that the stability as well as the bifurcation pictures is extremely sensitive to the value of

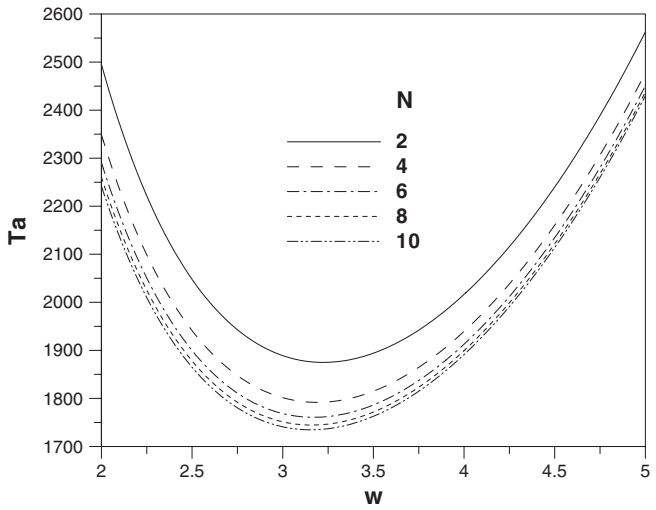

Figure 1. Assessment of convergence on the marginal stability picture for Newtonian flow. Truncation levels correspond to $N \in [2, 10]$.

Table I. Influence of higher-order modes on the critical Taylor number, Ta_c and corresponding wavenumber, w_c.

Number of modes N	Critical Taylor number Ta_c	Wavenumber w_c
2	1874.9	3.21
4	1791.8	3.18
6	1760.7	3.16
8	1744.5	3.15
10	1734.7	3.14

De (see below). In other words, rapid deviation from Newtonian behaviour occurs for small value of *De*. If *De* is small, η may be expressed as

$$\eta(\dot{\gamma}) = 1 + (1 - s)\left(\frac{n-1}{2}\right)(De\dot{\gamma})^2 = 1 + \alpha\dot{\gamma}^2 \tag{14}$$

where higher-order terms in *De* have been neglected, and $\alpha = (1 - s)((n - 1)/2)De^2$. In this case, Equations (13) are considerably simplified, and are explicitly given in the Appendix. The parameter α can then be used as a measure of non-Newtonian effects. Thus, in the limit $\alpha \to 0$, one can recover the expression for the Newtonian viscosity. It should be noted that α is negative (positive) for shear-thinning (shear-thickening) fluids.

3.1. Stability of the base flow

The stability analysis for a shear-thinning fluid is carried out around the CCF first. The analysis is based on the linearization of Equations (A1)–(A3) with $N = 6$. The marginal

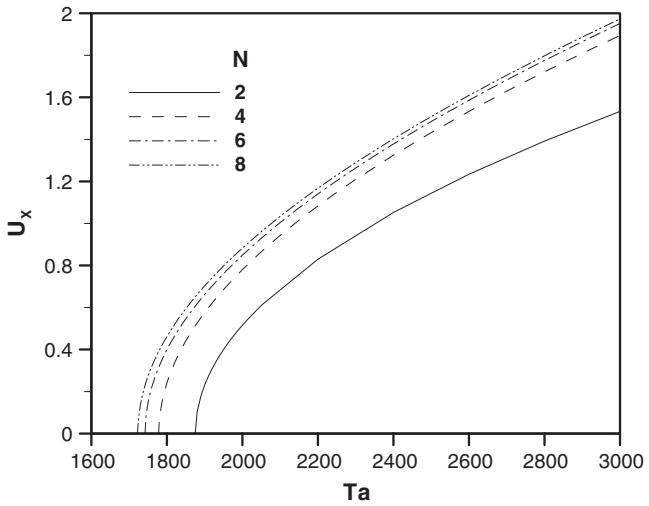

Figure 2. Assessment of convergence in the non-linear range (TVF) for a Newtonian fluid. Truncation levels correspond to $N \in [2, 8]$.

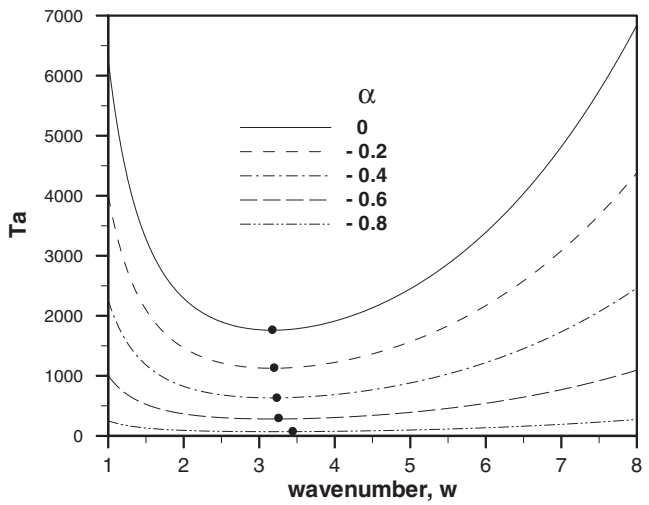

Figure 3. Influence of shear thinning on the marginal stability curves. Variations of the Ta as function of the wavenumber, w for $-0.8 \leqslant \alpha \leqslant 0.0$.

stability curves are depicted in Figure 3, where the critical Taylor number is plotted against the wave number for the range $\alpha \in [-0.8,\ 0.0]$. Note that the $\alpha = -1.0$ curve corresponding to an inviscid fluid. The figure shows that the critical Taylor number becomes smaller as shear-thinning effect increases (α decreases). In other words, it is found that shear thinning tends to destabilize the CCF. The value of the corresponding wavenumber, w_{m}, tends to increase

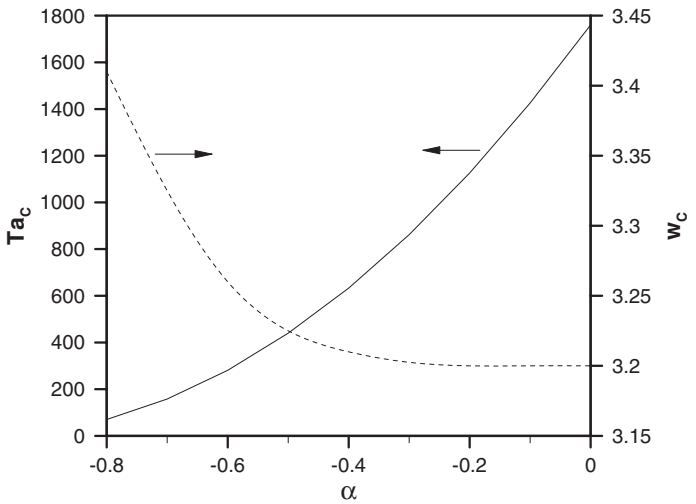

Figure 4. Influence of shear thinning on the critical Taylor number and corresponding wavenumber.

as α decreases. It is inferred from Figure 3 that shear thinning tends to precipitate the onset of axisymmetric Taylor vortices at any value of the wavenumber in the axial direction.

More explicitly, the critical Taylor number, Ta_c, and corresponding wavenumber, w_c, are plotted against α in Figure 4. There is a relatively sharp decrease in the value of Ta_c near the Newtonian limit. In contrast, the critical wavenumber remains insensitive to shear thinning until α reaches -0.4. At this point, w_c increases sharply, indicating an increase in cell number density in the TVF. The rate of decrease with shear thinning in the value of Ta at the onset of TVF depends strongly on the wavenumber. Figure 5 illustrates the influence of α and w on the onset of TVF. The rate of decrease of Ta with α increases with w. Thus, smaller cells tend to disappear relatively more quickly with shear thinning. In other words, the onset of TVF depends less strongly on α for the more shear-thinning fluid (see also the flattening of the marginal stability curves in Figure 3 as α decreases). As shear thinning increases the critical Taylor number decreases and reaches a zero value at $\alpha = -1$ (inviscid fluid). The recovery of the limit of zero critical Taylor number must of course be interpreted with caution as the limit $\alpha = -1$ is not within the range of validity of the present calculations.

Crumeyrolle *et al.* [37] investigated the instabilities appearing in the circular Couette flow with a dilute and semidilute solutions of high molecular weight polyethyleneoxide in water when the outer cylinder is kept at rest. They found that solutions with concentrations larger than 150 ppm exhibited a clear shear-thinning behaviour, which is well represented by the Carreau–Bird model. For dilute concentrations, the critical mode is the stationary and axisymmetric Taylor vortex flow, which bifurcates to time periodic wavy vortex flow for a higher Taylor number. For sufficiently semi-dilute solutions, the critical mode occurs in the form of standing waves, the frequency of which decreases with the Taylor number. The critical Taylor number increases for solutions without a shear-thinning effect and decreases for solutions exhibiting shear thinning. The comparison between their experimental results and the current theoretical calculations show a good agreement as illustrated in Figure 5, which are the

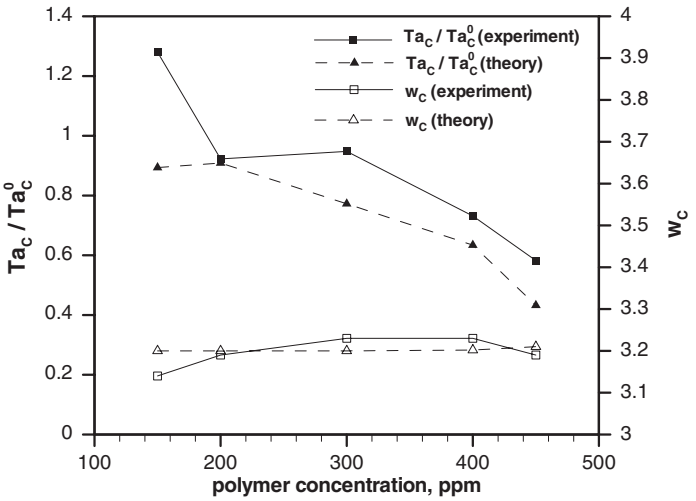

Figure 5. The plots of the reduced critical Taylor number, T, and the corresponding wavenumber, w_C, against the polymer concentration.

plots of the normalized critical Taylor number Ta_c/Ta_c^0 and corresponding critical wavenumber w_C against the polymer concentration of the solution. Here Ta_c^0 is the critical Taylor number corresponding to the onset of TVF for a Newtonian fluid.

3.2. *Steady-state solutions and bifurcation diagrams*

Similarly to the Newtonian equations, a trivial solution exists for Equations (A1)–(A3), which corresponds to the CCF or the origin in the phase space,

$$u_{1i}(x,z,t) = v_{1j}(x,z,t) = v_{0k}(x,z,t) = 0, \quad i,j,k = 1,2,\ldots,N \tag{15}$$

In addition, two non-trivial steady state solution branches exist, again similarly to Newtonian fluids. These two branches will be denoted by C_1 and C_2. In order to determine the steady-state branches, the Newton–Raphson method is used (IMSL-DNEQNF). However, despite the robustness of the Newton–Raphson method, and the fact that the non-linearities involved in the algebraic equations are only of the quadratic and cubic type, the bifurcation branches were found to be difficult to generate. The steady-state solution was found to be extremely sensitive to the initial guess. The guess had to be provided accurately enough for the method to converge. To circumvent this problem, one solution point had to be generated first by solving the time-dependent problem using the Runge–Kutta algorithm (IMSL-DIVPRK). Of course, this point must belong to the stable range of C_1 or C_2, and had to be obtained at a Taylor number below the critical value, Ta^h (see below). The solution was then used as the 'initial' guess for the Newton–Raphson program. With gradual increase of Ta, the solution branch was then generated. The starting point is usually difficult to obtain near the critical Taylor number, Ta_c, and was typically evaluated far ahead ($Ta \gg Ta_c$). The algebraic equations were then solved by increasing, and decreasing Ta from the starting point.

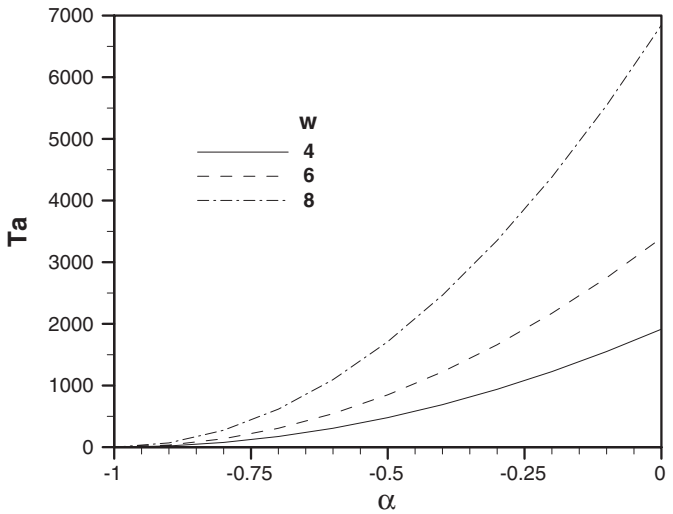

Figure 6. Influence of shear thinning on the value of the onset of TVF for various wavenumbers.

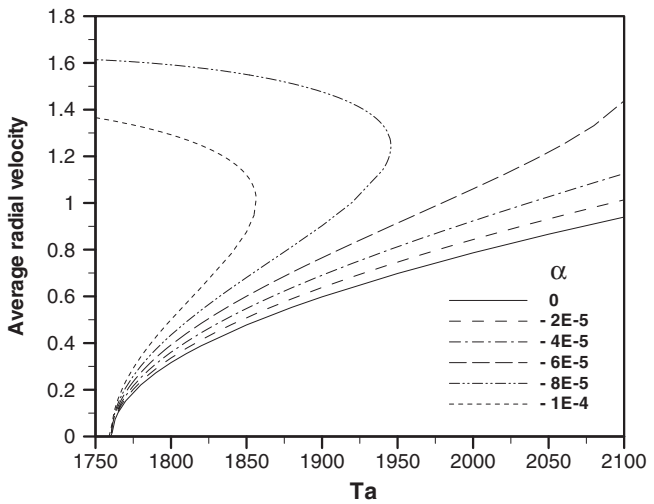

Figure 7. Influence of shear thinning on the bifurcation picture or the onset of TVF for $-0.0001 \leqslant \alpha \leqslant 0.0$ ($w = 3.2$). Note only one branch is shown (C_1) because of symmetry.

The bifurcation diagrams are shown in Figure 7 for a shear-thinning fluid, corresponding to the range $\alpha \in [-0.0001,\ 0.0]$, and $w = 3.2$. In general, the origin (in phase space) remains the only steady-state solution until Ta reaches the critical value, Ta_c, beyond which a non-trivial steady-state solution exists. Two additional fixed branches, C_1 and C_2, emerge, which correspond to the onset of Taylor vortices. Since each bifurcation diagram is symmetric, only one set of solution branches, C_1, is shown. It is recalled that, as α decreases from zero, the critical Taylor number, Ta_c, takes on smaller values, which indicates that shear thinning tends to destabilize the TCF. The figure depicts the behaviour of the radial velocity averaged

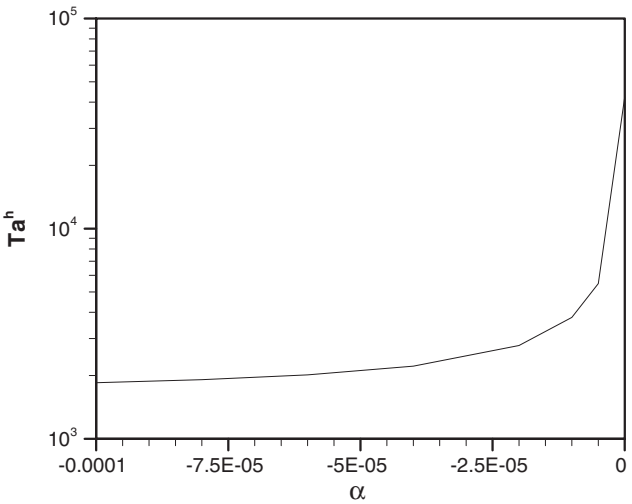

Figure 8. Influence of shear thinning on the loss of stability of TVF. The figure displays the dependence of Ta^h on α.

over $x \in [-\frac{1}{2}, \frac{1}{2}]$ and $z \in [0, \pi/w]$, which typically illustrates the dependence of the flow on the Taylor number. The figure indicates that shear thinning tends to accelerate the flow within the toroidal vortices. For a very small α value, the qualitative behaviour of the flow field remains the same as that for a Newtonian fluid, except perhaps that the velocity tends to grow faster with Ta, in the large Ta range.

Indeed, this acceleration in growth becomes evident as α decreases (from zero). The monotonic growth of the velocity gives way to a reversal in behaviour. Figure 7 indicates that, when shear-thinning effect is significant, the TVF is not maintained over an extended range of the Taylor number as for a Newtonian fluid. Instead, the TVF ceases to exist beyond a Ta value, which corresponds to a turning point in the bifurcation branch. The location of the turning point decreases significantly with shear thinning. Simultaneously, the overall flow amplitude begins to decrease as α decreases. Eventually, the onset of TVF becomes increasingly inhibited as shear-thinning effect increases. In general, the steady-state (TVF) loses its stability and will be discussed next.

3.3. Stability of the Taylor-vortex flow

Computations show that the non-trivial branches are typically linearly stable for a certain range $Ta > Ta_c$ near Ta_c. It is found, similarly to Newtonian fluids, that the stability of the TVF of shear-thinning fluids is lost through an inverse Hopf bifurcation at a critical Taylor number $Ta^h > Ta_c$. At this point, only an aperiodic solution seems to exist. The range of stability of the TVF is expected to be strongly influenced by shear thinning. Unlike Newtonian flow, the presence of shear thinning leads to a turning point in the branches C_1 and C_2. Figure 8 displays the dependence of Ta^h on α. Numerical values are also included in Table II for reference. The figure indicates that the loss of stability of the TVF is precipitated by shear thinning. More specifically, there is a rapid decrease in Ta^h as α decreases from the Newtonian

Table II. Numerical values of Ta^h corresponding to different α.

Shear-thinning effect α	Critical Taylor number Ta^h
0.0	42330
−0.000005	5480
−0.00001	3780
−0.00002	2779
−0.00004	2216
−0.00006	2015
−0.00008	1912
−0.00010	1849

limit. However, the value of the critical Taylor number appears to level off in the low α range. Both Figures 7 and 8 indicate that the turning points are indeed bifurcation points. This is particularly obvious from the curves corresponding to $\alpha = -0.00008$ and -0.0001.

4. CONCLUSION

The effect of shear thinning on the stability of rotating flow is investigated in the narrow-gap limit. A dynamical system approach is derived using Fourier and Chandrasekhar orthonormal functions to examine the impact of shear thinning on finite amplitude Taylor vortex flow. Linear stability analysis indicates that the onset of TVF is precipitated by shear thinning. The presence of shear thinning leads to additional nonlinearities in the dynamical system. The effect of shear thinning is significant even close to the Newtonian limit. Although the TVF emerges via the usual supercritical bifurcation, the corresponding steady-state branches exhibit a turning point not observed for Newtonian flow. It is found that the TVF loses its stability at a Taylor number coinciding with the turning point. Comparison with experimental results on critical Taylor and wave numbers show good agreement with the current theoretical predictions.

APPENDIX. SMALL *De* FORMULATION

In this appendix, the governing equations in the limit of small *De* are deduced from Equation (13), which are written as ($p = 1, 2, \ldots, N$)

$$\begin{aligned} v_{0p,t} = {} & A_1^p \sum_{k=1}^{N}\sum_{i=1}^{N} v_{1k}u_{1i} + (1+3\alpha)A_2^p \sum_{j=1}^{N} v_{0j} + \alpha\left(A_3^p \sum_{j=1}^{N}\sum_{k=1}^{N}\sum_{i=1}^{N} v_{0j}v_{0k}v_{0i}\right. \\ & + A_4^p \sum_{j=1}^{N}\sum_{k=1}^{N}\sum_{i=1}^{N} v_{1j}v_{1k}v_{0i} + A_5^p \sum_{j=1}^{N}\sum_{i=1}^{N} v_{0j}v_{0i} + A_6^p \sum_{j=1}^{N}\sum_{k=1}^{N}\sum_{i=1}^{N} u_{1j}u_{1k}v_{0i} \\ & \left. + A_7^p \sum_{j=1}^{N}\sum_{i=1}^{N} v_{1j}v_{1i} + A_8^p \sum_{j=1}^{N}\sum_{i=1}^{N} v_{1j}u_{1i}\right) \end{aligned} \tag{A1}$$

$$v_{1p,t} = B_1^p \sum_{k=1}^{N}\sum_{i=1}^{N} v_{0k}u_{1i} + u_{1p} - w^2(1+\alpha)v_{1p} + (1+3\alpha)B_2^p \sum_{j=1}^{N} v_{1j}$$
$$+\alpha\left(B_3^p \sum_{j=1}^{N}\sum_{i=1}^{N} v_{1j}v_{0i} + B_4^p \sum_{j=1}^{N}\sum_{k=1}^{N}\sum_{i=1}^{N} v_{0j}v_{1k}v_{0i} + B_5^p \sum_{j=1}^{N}\sum_{k=1}^{N}\sum_{i=1}^{N} v_{1j}v_{1k}v_{1i}\right.$$
$$\left. + B_6^p \sum_{j=1}^{N}\sum_{k=1}^{N}\sum_{i=1}^{N} u_{1j}u_{1k}v_{1i}\right) \tag{A2}$$

$$C_1^p \sum_{i=1}^{N} u_{1i,t} = 2w^2 Ta\left(C_2^p \sum_{k=1}^{N}\sum_{i=1}^{N} v_{0k}v_{1i} + C_3^p \sum_{k=1}^{N} v_{1k}\right)$$
$$-(w^4 + \beta_p^4)(1+\alpha)u_{1p} + 2\alpha w^2 C_4^p \sum_{i=1}^{N} u_{1i} + \alpha\left(C_5^p \sum_{j=1}^{N}\sum_{i=1}^{N} v_{0j}u_{1i}\right.$$
$$\left. + C_6^p \sum_{j=1}^{N}\sum_{k=1}^{N}\sum_{i=1}^{N} v_{0j}v_{0k}u_{1i} + C_7^p \sum_{j=1}^{N}\sum_{k=1}^{N}\sum_{i=1}^{N} v_{1j}v_{1k}u_{1i} + C_8^p \sum_{j=1}^{N}\sum_{k=1}^{N}\sum_{i=1}^{N} u_{1j}u_{1k}u_{1i}\right) \tag{A3}$$

where $\beta_p = \begin{cases} \mu_p & p \text{ even} \\ \lambda_p & p \text{ odd} \end{cases}$ are the Chandrasekhar constants [41].

$A_1^p, \ldots, A_8^p, B_1^p, \ldots, B_6^p$, and $C_1^p, \ldots, C_8^p$ are constant coefficients that are given by

$$A_1^p = -\frac{1}{2}(\langle \Phi_{k,x}\Phi_i\Phi_p\rangle + \langle \Phi_k\Phi_{i,x}\Phi_p\rangle)$$
$$A_2^p = \langle \Phi_{j,xx}\Phi_p\rangle$$
$$A_3^p = 3\langle \Phi_{k,x}\Phi_{j,x}\Phi_{i,xx}\Phi_p\rangle$$
$$A_4^p = \frac{9}{2}\langle \Phi_{k,x}\Phi_{j,x}\Phi_{i,xx}\Phi_p\rangle + \frac{w^2}{2}\langle \Phi_k\Phi_j\Phi_{i,xx}\Phi_p\rangle + w^2\langle \Phi_k\Phi_{j,x}\Phi_{i,x}\Phi_p\rangle$$
$$A_5^p = -6\langle \Phi_{j,x}\Phi_{i,xx}\Phi_p\rangle$$
$$A_6^p = \frac{1}{2w^2}\langle \Phi_{k,xx}\Phi_{j,xx}\Phi_{i,xx}\Phi_p\rangle + \langle \Phi_k\Phi_{j,xx}\Phi_{i,xx}\Phi_p\rangle + \frac{w^2}{2}\langle \Phi_k\Phi_j\Phi_{i,xx}\Phi_p\rangle$$
$$+ \frac{1}{w^2}\langle \Phi_{k,xx}\Phi_{j,xxx}\Phi_{i,x}\Phi_p\rangle + \langle \Phi_{k,x}\Phi_{j,xx}\Phi_{i,x}\Phi_p\rangle + \langle \Phi_k\Phi_{j,xxx}\Phi_{i,x}\Phi_p\rangle$$
$$+ w^2\langle \Phi_k\Phi_{j,x}\Phi_{i,x}\Phi_p\rangle$$

$$A_7^p = -3\langle \Phi_{j,x}\Phi_{i,xx}\Phi_p\rangle - w^2\langle \Phi_j\Phi_{i,x}\Phi_p\rangle$$

$$A_8^p = \frac{1}{w^2}\langle \Phi_{j,xx}\Phi_{i,xxx}\Phi_p\rangle + \langle \Phi_{j,x}\Phi_{i,xx}\Phi_p\rangle + \langle \Phi_j\Phi_{i,xxx}\Phi_p\rangle + w^2\langle \Phi_j\Phi_{i,x}\Phi_p\rangle$$

$$B_1^p = -\langle \Phi_{k,x}\Phi_i\Phi_p\rangle$$

$$B_2^p = \langle \Phi_{i,xx}\Phi_p\rangle$$

$$B_3^p = -6\langle \Phi_{k,xx}\Phi_{i,x}\Phi_p\rangle - 6\langle \Phi_{k,x}\Phi_{i,xx}\Phi_p\rangle + 2w^2\langle \Phi_k\Phi_{i,x}\Phi_p\rangle$$

$$B_4^p = 6\langle \Phi_{k,x}\Phi_{j,x}\Phi_{i,xx}\Phi_p\rangle + 3\langle \Phi_{k,xx}\Phi_{j,x}\Phi_{i,x}\Phi_p\rangle - w^2\langle \Phi_k\Phi_{j,x}\Phi_{i,x}\Phi_p\rangle$$

$$B_5^p = \frac{9}{4}\langle \Phi_{k,x}\Phi_{j,x}\Phi_{i,xx}\Phi_p\rangle + \frac{w^2}{4}\langle \Phi_{k,x}\Phi_{j,x}\Phi_i\Phi_p\rangle - \frac{3w^4}{4}\langle \Phi_k\Phi_j\Phi_i\Phi_p\rangle + \frac{w^2}{4}\langle \Phi_k\Phi_j\Phi_{i,xx}\Phi_p\rangle$$

$$B_6^p = \frac{1}{4w^2}\langle \Phi_{k,xx}\Phi_{j,xx}\Phi_{i,xx}\Phi_p\rangle + \frac{1}{2}\langle \Phi_k\Phi_{j,xx}\Phi_{i,xx}\Phi_p\rangle + \frac{w^2}{4}\langle \Phi_k\Phi_j\Phi_{i,xx}\Phi_p\rangle + \frac{1}{2w^2}\langle \Phi_{k,xx}\Phi_{j,xxx}\Phi_{i,x}\Phi_p\rangle + \frac{1}{2}\langle \Phi_{k,x}\Phi_{j,xx}\Phi_{i,x}\Phi_p\rangle + \frac{1}{2}\langle \Phi_k\Phi_{j,xxx}\Phi_{i,x}\Phi_p\rangle + \frac{w^2}{2}\langle \Phi_k\Phi_{j,x}\Phi_{i,x}\Phi_p\rangle - \frac{3w^4}{4}\langle \Phi_k\Phi_j\Phi_i\Phi_p\rangle - \frac{3w^2}{2}\langle \Phi_k\Phi_{j,xx}\Phi_i\Phi_p\rangle - \frac{3}{4}\langle \Phi_{k,xx}\Phi_{j,xx}\Phi_i\Phi_p\rangle$$

$$C_1^p = w^2\delta_{ip} - \langle \Phi_{i,xx}\Phi_p\rangle$$

$$C_2^p = \langle \Phi_j\Phi_k\Phi_p\rangle$$

$$C_3^p = \langle (0.5-x)\Phi_k\Phi_p\rangle$$

$$C_4^p = \langle \Phi_{i,xx}\Phi_p\rangle$$

$$C_5^p = -4w^2\langle \Phi_{j,x}\Phi_{i,xx}\Phi_p\rangle + 2(w^4+\beta_i^4)\langle \Phi_{j,x}\Phi_i\Phi_p\rangle - 4w^2\langle \Phi_{j,xx}\Phi_{i,x}\Phi_p\rangle + 4\langle \Phi_{j,xx}\Phi_{i,xxx}\Phi_p\rangle + 2\langle \Phi_{j,xxx}\Phi_{i,xx}\Phi_p\rangle + 2w^2\langle \Phi_{j,xxx}\Phi_i\Phi_p\rangle$$

$$C_6^p = w^2\langle \Phi_{j,x}\Phi_{k,x}\Phi_{i,xx}\Phi_p\rangle + w^2\langle \Phi_{j,xx}\Phi_{k,x}\Phi_{i,xx}\Phi_p\rangle + 4w^2\langle \Phi_{j,x}\Phi_{k,xx}\Phi_{i,x}\Phi_p\rangle - (w^4+\beta_i^4)\langle \Phi_{j,x}\Phi_{k,x}\Phi_i\Phi_p\rangle - 4\langle \Phi_{j,x}\Phi_{k,xx}\Phi_{i,xxx}\Phi_p\rangle - 2\langle \Phi_{j,xx}\Phi_{k,xx}\Phi_{i,xx}\Phi_p\rangle$$

$$
\begin{aligned}
&- 2\langle \Phi_{j,x}\Phi_{k,xxx}\Phi_{i,xx}\Phi_p\rangle - 2w^2\langle \Phi_{j,xx}\Phi_{k,xx}\Phi_i\Phi_p\rangle \\
&- 2w^2\langle \Phi_{j,x}\Phi_{k,xxx}\Phi_i\Phi_p\rangle \\
C_7^p = &\frac{3w^2}{2}\langle \Phi_{j,x}\Phi_{k,x}\Phi_{i,xx}\Phi_p\rangle - \frac{w^4}{2}\langle \Phi_j\Phi_k\Phi_{i,xx}\Phi_p\rangle \\
&- \left(\frac{7w^4}{4} + \frac{3\beta_i^4}{4}\right)\langle \Phi_{j,x}\Phi_{k,x}\Phi_i\Phi_p\rangle - \frac{3w^2}{4}(w^4+\beta_i^4)\langle \Phi_j\Phi_k\Phi_i\Phi_p\rangle \\
&+ 5w^2\langle \Phi_{j,x}\Phi_{k,xx}\Phi_{i,x}\Phi_p\rangle - w^4\langle \Phi_j\Phi_{k,x}\Phi_{i,x}\Phi_p\rangle \\
&- \langle \Phi_{j,x}\Phi_{k,xx}\Phi_{i,xxx}\Phi_p\rangle - 3w^2\langle \Phi_j\Phi_{k,x}\Phi_{i,xxx}\Phi_p\rangle \\
&- \frac{1}{2}\langle \Phi_{j,x}\Phi_{k,xxx}\Phi_{i,xx}\Phi_p\rangle - \frac{3w^2}{2}\langle \Phi_j\Phi_{k,xx}\Phi_{i,xx}\Phi_p\rangle \\
&- \frac{w^2}{2}\langle \Phi_{j,xx}\Phi_{k,xx}\Phi_i\Phi_p\rangle - \frac{w^2}{2}\langle \Phi_{j,x}\Phi_{k,xxx}\Phi_i\Phi_p\rangle \\
&- \frac{3w^2}{2}\langle \Phi_j\Phi_{k,xx}\Phi_i\Phi_p\rangle \\
C_8^p = &-2\langle \Phi_{j,xx}\Phi_{k,xx}\Phi_{i,xx}\Phi_p\rangle - \frac{1}{4w^2}(19w^4+9\beta_i^4)\langle \Phi_j\Phi_{k,xx}\Phi_{i,xx}\Phi_p\rangle \\
&- \left(\frac{7w^4}{2} + \frac{9\beta_i^4}{2}\right)\langle \Phi_j\Phi_{k,xx}\Phi_i\Phi_p\rangle - \frac{3w^2}{4}(w^4+3\beta_i^4)\langle \Phi_j\Phi_k\Phi_i\Phi_p\rangle \\
&- 7\langle \Phi_{j,x}\Phi_{k,xx}\Phi_{i,xxx}\Phi_p\rangle - \left(2w + \frac{w^2}{2}\right)\langle \Phi_{j,x}\Phi_{k,xx}\Phi_{i,x}\Phi_p\rangle \\
&- (5w^2+2w)\langle \Phi_j\Phi_{k,x}\Phi_{i,xxx}\Phi_p\rangle - \frac{5w^4}{2}\langle \Phi_j\Phi_{k,x}\Phi_{i,x}\Phi_p\rangle \\
&- \frac{9}{2k^2}\langle \Phi_{j,xx}\Phi_{k,xxx}\Phi_{i,xxx}\Phi_p\rangle - \frac{9}{2}\langle \Phi_{j,xxx}\Phi_{k,xxx}\Phi_i\Phi_p\rangle
\end{aligned}
$$

where, $\langle\ \rangle = \int_{-0.5}^{0.5} \mathrm{d}x$.

REFERENCES

1. Sell GR, Foias C, Temam R. *Turbulence in Fluid Flows*: *A Dynamical Systems Approach.* Springer: New York, 1993.
2. Berge P, Pomeau Y, Vidal C. *Order within Chaos.* Hermann and John Wiley & Sons: Paris, 1984.
3. Kuhlmann H. Model for Taylor–Couette flow. *Physical Review* A 1985; **32**(3):1703–1707.
4. Kuhlmann H, Roth D, Lücke M. Taylor flow and harmonic modulation of the driving force. *Physical Review* A 1988; **39**(2):745–762.

5. Khayat RE. Chaos and overstability in the thermal convection of viscoelastic fluids. *Journal of Non-Newtonian Fluid Mechanics* 1994; **53**:227–255.
6. Khayat RE. Fluid elasticity and transition to chaos in thermal convection. *Physical Review* E 1995; **51**(1): 380–399.
7. Khayat RE. Nonlinear overstability in the thermal convection of viscoelastic fluids. *Journal of Non-Newtonian Fluid Mechanics* 1995; **58**:331–356.
8. Khayat RE. Chaos in the thermal convection of weakly shear-thinning fluids. *Journal of Non-Newtonian Fluid Mechanics* 1996; **63**:153–178.
9. Khayat RE. Onset of Taylor vortices and chaos in viscoelastic fluids. *Physics of Fluids* 1995; **7**(9):2191–2219.
10. Khayat RE. Low-dimensional approach to nonlinear overstability of purely elastic Taylor-vortex flow. *Physical Review Letters* 1997; **78**(26):4918–4921.
11. Khayat RE. Finite-amplitude Taylor-vortex flow of viscoelastic fluids. *Journal of Fluid Mechanics* 1999; **400**: 33–58.
12. Ashrafi N, Khayat RE. Shear-thinning induced chaos in Taylor–Couette flow. *Physical Review* E 2000; **61**(2):1455–1467.
13. Ashrafi N, Khayat RE. A low-dimensional approach to nonlinear plane-Couette flow of viscoelastic fluids. *Physics of Fluids* 2000; **12**(2):345–365.
14. Khayat RE, Ashrafi N. Nonlinear stability and bifurcation in plane-Poiseuille flow of viscoelastic fluids. *ASME Journal of Applied Mechanics* 2000; **67**(4):834–837.
15. Muller SJ, Shaqfeh ESG, Larson RG. Experimental study of the onset of oscillatory instability in viscoelastic Taylor–Couette flow. *Journal of Non-Newtonian Fluid Mechanics* 1993; **46**:315–330.
16. Bird RB, Armstrong RC, Hassager O. *Dynamics of Polymeric Liquids* (2nd edn), vol. 1. Wiley: New York, 1987.
17. Larson RG, Shaqfeh ESG, Muller SJ. A purely elastic instability in Taylor–Couette flow. *Journal of Fluid Mechanics* 1990; **218**:573–600.
18. Baumert BM, Muller SJ. Flow visualization of the elastic Taylor–Couette flow in Boger fluids. *Rheologica Acta* 1995; **34**:147–157.
19. Baumert BM, Muller SJ. Axisymmetric and non-axisymmetric elastic and inertio-elastic instabilities in Taylor–Couette flow. *Journal of Non-Newtonian Fluid Mechanics* 1999; **83**:33–69.
20. Ashurst WT, Hoover WG. Dense-fluid shear viscosity via nonequilibrium molecular dynamics. *Physical Review* A 1975; **11**(2):658–678.
21. Erpenbeck JJ. Non-equilibrium molecular dynamics calculations of the shear viscosity of hard spheres. *Physica* A 1983; **118**(1):144–156.
22. Heyes DM. Shear thinning of the Lennard-Jones fluid by molecular dynamics. *Physica* A 1985; **133**(3): 473–496.
23. Eu BC. *Kinetic Theory and Irreversible Thermodynamics.* Wiley: New York, 1992.
24. Bhattacharya DK, Eu BC. Theory of dynamic shear viscosity and normal stress coefficients of dense fluids. *Molecular Physics* 1986; **59**:1145–1164.
25. Evans DJ. Rheological properties of simple fluids by computer simulation. *Physical Review* A 1981; **23**(4):1988 –1997.
26. Khayat RE, Eu BC. Nonlinear transport processes and fluid dynamics: cylindrical Couette flow of Lennard-Jones fluids. *Physical Review* A 1988; **38**(5):2492–2507.
27. Khayat RE, Eu BC. Generalized hydrodynamics, normal-stress effects and velocity slips in the cylindrical Couette flow of Lennard-Jones fluids. *Physical Review* A 1989; **39**(2):728–744.
28. Khayat RE, Eu BC. Generalized hydrodynamics and Reynolds-number dependence of steady-flow properties in the cylindrical Couette flow of Lennard-Jones fluids. *Physical Review* A 1989; **40**(2):946–958.
29. Khayat RE, Eu BC. Extended irreversible thermodynamics, generalized hydrodynamics, kinetic theory and rheology. *Rheologica Acta* 1991; **30**:204–212.
30. Grad H. On the kinetic theory of rarified gases. *Communications on Pure and Applied Mathematics* 1949; **2**:331–407.
31. Larson RG. Instabilities in viscoelastic flows. *Rheologica Acta* 1992; **31**:213–263.
32. Veronis G. Motions at subcritical values of the Rayleigh number in a rotating fluid. *Journal of Fluid Mechanics* 1966; **24**:545–554.
33. Shirer HN, Wells R. *Mathematical Structure of the Singularities at the Transition between Steady States in Hydrodynamic Systems.* Springer: Heidelberg, 1980.
34. Yahata H. Temporal development of the Taylor vortices in a rotating fluid. I. *Progress of Theoretical Physics* 1978; **59**(5):1755–1756.
35. Yahata H. Temporal development of the Taylor vortices in a rotating fluid. II. *Progress of Theoretical Physics* 1979; **61**(3):791–800.
36. Yorke JA, Yorke ED. Chaotic behaviour and fluid dynamics. In *Hydrodynamic Instabilities and the Transition to Turbulence*, Swinney HL, Gollub JP (eds), Topics in Applied Physics, vol. 45. Springer: Berlin, 1981; 77–96.

37. Crumeryrolle O, Mutabazi I, Grisel M. Experimental study of inertioelastic Couette–Taylor instability modes in dilute and semidilute polymer solutions. *Physics of Fluids* 2002; **14**(5):1681–1688.
38. Yi M, Kim C. Experimental studies on the Taylor instability of dilute polymer solutions. *Journal of Non-Newtonian Fluid Mechanics* 1997; **72**:113–139.
39. Sinevic V, Kuboi R, Nienow AW. Power numbers, Taylor numbers and Taylor vortices in viscous Newtonian and non-Newtonian fluids. *Chemical Engineering Science* 1986; **41**(11):2915–2923.
40. Escudier MP, Gouldson IW, Jones DM. Taylor vortices in Newtonian and shear-thinning liquids. *Proceedings of the Royal Society of London* A 1995; **449**:155–176.
41. Chandrasekhar S. *Hydrodynamic and Hydromagnetic Stability.* Dover Publications: New York, 1961.

